Ray-wave correspondence in the nonlinear description of stadium-cavity lasers

Susumu Shinohara,[1] Takahisa Harayama,[1] Hakan E. Türeci,[2] and A. Douglas Stone[2]
[1]*Department of Nonlinear Science, ATR Wave Engineering Laboratories, 2-2-2 Hikaridai, Seika-cho, Soraku-gun, Kyoto 619-0288, Japan*
[2]*Department of Applied Physics, Yale University, P.O. Box 208284, New Haven, Connecticut 06520-8284, USA*
(Received 18 March 2006; published 26 September 2006)

We show that the solution of fully nonlinear lasing equations for stadium cavities exhibits a highly directional emission pattern. This directionality can be well explained by a ray-dynamical model, where the dominant ray-escape dynamics is governed by the unstable manifolds of the unstable short periodic orbits for the stadium cavity. Investigating the cold-cavity modes relevant for the lasing, we found that all of the high-Q modes have the emission directionality corresponding to that of the ray-dynamical model.

DOI: 10.1103/PhysRevA.74.033820 PACS number(s): 42.55.Sa, 05.45.Mt, 42.60.Da

Establishing a correspondence between the ray (or classical) picture and the wave (or quantum) picture has been a fundamental problem in the field of wave (or quantum) chaos [1]. One encounters this problem when trying to understand the emission properties from two-dimensional (2D) microcavity lasers. In such lasers, as a way to extract highly directional emission, it has been proposed to deform the cavity shape smoothly from perfect circularity [2–6]. The result is that rays start to exhibit a variety of dynamics from integrable to strongly chaotic, which is tunable by the deformation.

The ray picture has been providing a simple and intuitive method to explain experimental observations of emission directionality. For instance, emission directionality has been associated with the existence of a periodic orbit with a particular geometry [6,7], drastic shape dependence of emission directionality has been successfully explained by the difference of phase-space structure [8], and the far-field intensity patterns have been closely reproduced by ray-tracing simulations [8–10].

Among various cavity shapes, the stadium is a simple geometry for which ray dynamics has been rigorously proven to become strongly chaotic [11]. For almost all initial conditions, a ray trajectory explores the entire phase space uniformly. Even for such a strongly chaotic cavity, if one considers refractive emission of light due to the dielectric nature of the cavity, the emission pattern can become highly directional. Namely, strongly chaotic dynamics and highly directional emission are compatible, as was demonstrated by Schwefel *et al.* [8], who associated this property with escape dynamics dominated by flow in phase space along the unstable manifolds of the unstable short periodic orbits of a chaotic system.

In this paper, we report further evidence for the ability of a ray-dynamical model to describe the lasing states of two-dimensional microcavities. Earlier work has focused on establishing a relationship between the ray model and a few quasibound-state solutions of the linear wave equation, without pumping or gain. Which modes to choose for comparison in this case has an intrinsic arbitrariness, although plausibility arguments can be made based on their Q values. Here we show that the solution of the full nonlinear lasing equations for a stadium cavity, uniquely determined by the pumping conditions, has highly directional emission in good agreement with the ray model. This is one of the first pieces of evidence that the multimode solutions of nonlinear wave equations can be understood in terms of the classical limit of its linear counterpart.

Firstly, it is shown that a ray model for the stadium cavity exhibits highly directional far-field emission. In this paper, we fix the aspect ratio of the stadium to $a/r=6/7$, where r and a are the radius of the semicircles and the half-length of the straight segments, respectively [Fig. 1(a)]. In the ray model, the appearance of strong directionality depends heavily on the value of the refractive index of the cavity n_{in}. We set $n_{in}=1.49$, which corresponds to the index for polymer cavities [8].

The ray model is constructed on the basis of Snell's and Fresnel's laws [3–5,8–10,12–14]. Inside the cavity, the dynamics of a ray is viewed as the motion of a point particle moving freely except for reflections at the cavity boundary. The ray dynamics can be reduced to a two-dimensional area-preserving mapping by introducing the Birkhoff coordinates $(s,\sin\phi)$, where s is the arc length along the cavity boundary and ϕ is the angle of incidence [Fig. 1(a)]. Taking into account the dielectric nature of the cavity, we consider the emission of rays to the outside of the cavity, which is done in the following manner. Each ray is initially assigned a certain amount of intensity. This intensity decreases whenever a ray collides with the cavity boundary, where the amount of the emitted-ray intensity is determined by Fresnel's law, while the ray's emission angle is given by Snell's law.

In the ray model simulations, we prepare the initial ensemble of rays to be uniformly distributed in the phase space spanned by the Birkhoff coordinates. After some transient, the total intensity of rays inside the cavity decreases exponentially as a function of time [14]. In such a stationary regime, we measure the intensity distribution for the emitted rays $I(s,\sin\phi)$.

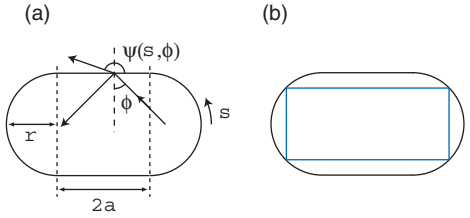

FIG. 1. (Color online) (a) Geometry of the stadium cavity and (b) the rectangular unstable periodic orbit.

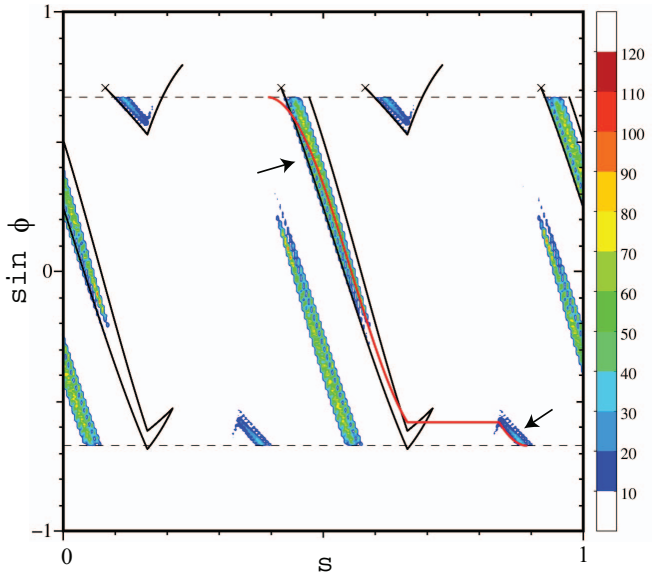

FIG. 2. (Color) Ray model simulation: intensity distribution of emitted rays $I(s,\sin\phi)$. The black solid curves are the unstable manifolds of the rectangular unstable periodic orbit marked by $\times$. The red curve is a set of points giving the far-field emission at $\theta=210°$. The black dashed lines indicate the critical lines for total internal reflection defined by $\sin\phi=\pm 1/n_{in}$.

The qualitative explanation for strong emission directionality in such a chaotic system was given by Schwefel *et al.* [8]; the unstable short periodic orbits act like anisotropic "scattering centers" in phase space, causing directional flow along their unstable manifolds until the critical angle for escape is reached. For shapes like the stadium there exists a "line of constant far field" corresponding to the set of values of the angle of incidence ϕ and angular position on the boundary s at which a ray refracts in the same far-field angular direction. The line of constant far field closest to the unstable manifold then predicts the dominant emission directionality. Note that all of the relevant short orbits have closely nested unstable manifolds so this gives a unique prediction [8]. The data in Fig. 2 are in agreement with this picture. In Fig. 2, $I(s,\sin\phi)$ is plotted overlaid with the unstable manifolds of the rectangular unstable periodic orbit [Fig. 1(b)] located near the critical line for total internal reflection, i.e., $\sin\phi=1/n_{in}$. For $n_{in}=1.49$, we see that high escape intensity regions consist of narrow stripes corresponding closely to the unstable manifolds, and that two stripes of high intensity (marked by arrows) are almost parallel to the constant far-field curve for $\theta=210°$ (red curve), where the angular coordinate θ is defined as the counterclockwise angle from the x axis. By the fourfold symmetry of the stadium each of the other stripes is parallel to one of the curves for $\theta=30°$, 150°, and 330°, giving a fourfold symmetric directional emission pattern peaked around these angular directions. We plot the far-field intensity pattern $\mathcal{F}(\theta)$ in Fig. 3, which can be calculated from the intensity distribution $I(s,\sin\phi)$ via $\mathcal{F}(\theta)=\int\int ds\, d(\sin\phi) I(s,\sin\phi)\delta[\psi(s,\phi)-\theta]$, where $\psi(s,\phi)$ is the emission angle (measured from the x axis) at s for a ray with the angle of incidence ϕ [13]. This is the result of the ray model.

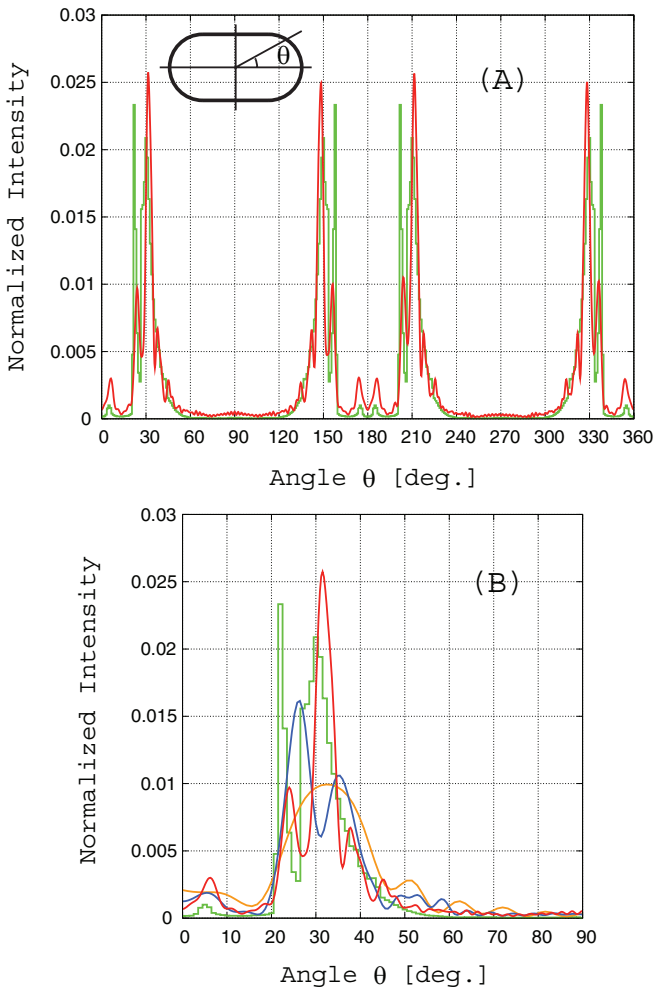

FIG. 3. (Color) The far-field intensity patterns for the stadium cavity with $n_{in}=1.49$. (A) The ray model (green) vs the Schrödinger-Bloch model (red). (B) The ray model (green) vs the Schrödinger-Bloch model (red, $r=67.77$; blue, $r=33.88$; orange, $r=16.94$).

Now, we investigate whether one can find the same emission directionality for the lasing states for this cavity. We describe the light field by the Maxwell equations, and assume that the active medium consists of two-level atoms obeying the Bloch equations. In the description using the Maxwell and Bloch equations, the field variables oscillate rapidly at a frequency close to the transition frequency ω_0 of the two-level atoms. To perform the long-term time evolutions necessary to obtain stationary lasing solutions, we employ the Schrödinger-Bloch (SB) model, which describes the time evolution of the slowly varying envelopes of the field variables [15–18]. The SB model is given by

$$\frac{\partial E}{\partial t}=\frac{i}{2}\left(\nabla^2+\frac{n^2}{n_{in}^2}\right)E-\alpha E+\mu\rho, \tag{1}$$

$$\frac{\partial \rho}{\partial t}=-\gamma_\perp\rho+\kappa W E, \tag{2}$$

$$\frac{\partial W}{\partial t}=-\gamma_\parallel(W-W_\infty)-2\kappa(E\rho^*+E^*\rho), \tag{3}$$

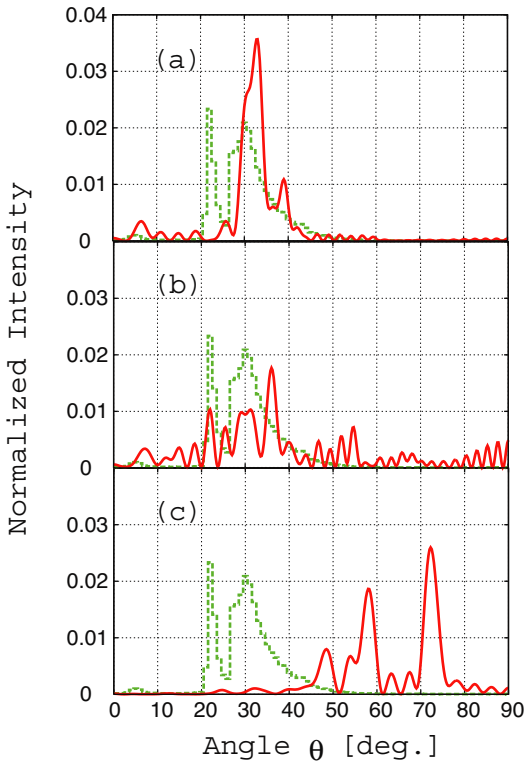

FIG. 4. (Color online) The far-field patterns for the cold-cavity modes with even-even parity (solid line) and for the ray model (dashed line). (a) $\xi=-0.007\,054-0.002\,507i$, (b) $\xi=0.009\,670-0.005\,197i$, (c) $\xi=-0.006\,299-0.010\,132i$. Because of the pattern's symmetry, only the data in the first quadrant are shown.

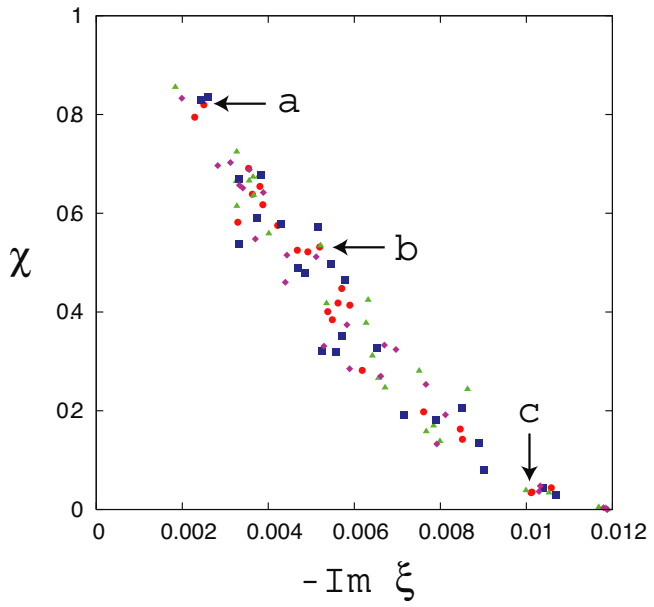

FIG. 5. (Color online) The dependence of χ (far-field emission strength around $\theta=30°$) on the loss rate $-\mathrm{Im}\,\xi$ for even-even (circle), even-odd (triangle), odd-even (square), and odd-odd (diamond) modes. The modes corresponding to the far-field patterns in Fig. 4 are marked with arrows.

where $E(x,y,t)$ and $\rho(x,y,t)$ are the slowly varying envelopes of the TM electric field and that of the polarization field, respectively, and $W(x,y,t)$ is the population-inversion component. The refractive index $n(x,y)$ is $n_{in}(=1.49)$ inside the cavity and 1.0 outside it, and the linear-absorption coefficient $\alpha(x,y)$ is $\alpha_L(=\text{const})$ inside the cavity and zero outside it. Space and time are made dimensionless by the scale transformations $(n_{in}\omega_0 x/c, n_{in}\omega_0 y/c)\to(x,y)$ and $\omega_0 t\to t$. $\gamma_\perp$ and $\gamma_\parallel$ are phenomenological relaxation rates, κ and μ are the coupling strength between the light field and the active medium, and W_∞ represents the pumping strength.

Unless otherwise mentioned, the cavity size is $r=67.77$, for which the perimeter length of the stadium becomes about 105 times as large as the light wavelength inside the cavity, i.e., $\lambda_{in}=2\pi$. The other parameter values are set as follows: $W_\infty=0.01$, $\gamma_\perp=10^{-2}$, $\gamma_\parallel=10^{-5}$, $\alpha_L=10^{-3}$, $\kappa=0.5$, $\mu=\pi/n_{in}^2$. For the above choice of the parameter values, around 100 cavity modes have positive linear gain. For such a condition, there occur complicated interactions between the modes, such as mode pulling and mode pushing, that generally yield a multimode lasing solution [16,17]. We are interested in the far-field patterns arising from these multimode lasing solutions; we now formulate a convenient method for finding this quantity on the basis of the field data just outside the cavity.

Using the Wiener-Khinchin theorem, one can write the time-averaged light intensity as

$$\bar{\mathcal{I}}(\boldsymbol{r},t)=\int d\omega \lim_{T\to\infty}\frac{2\pi}{T}|E_T(\boldsymbol{r},\omega)|^2, \tag{4}$$

where $E_T(\boldsymbol{r},\omega)=\frac{1}{2\pi}\int_{-T/2}^{T/2}E(\boldsymbol{r},t)e^{i\omega t}$. In the far-field regime ($r\gg 1$), we obtain $|E_T(\boldsymbol{r},\omega)|^2=|f_T(\theta,\omega)|^2/r$, where the amplitude $f_T(\theta,\omega)$ is given by

$$f_T(\theta,\omega)=\frac{1+i}{4\sqrt{\pi k}}\oint_{\mathcal{C}} ds e^{-ik(\boldsymbol{e}\cdot\boldsymbol{r}_s)}\boldsymbol{n}_s\cdot(ik\boldsymbol{e}+\boldsymbol{\nabla})E_T(\boldsymbol{r}_s,\omega), \tag{5}$$

with $k=\sqrt{1/n_{in}^2+2\omega}$. The integration is performed along a closed curve $\mathcal{C}$ encircling the cavity, $\boldsymbol{r}_s$ denotes a point on $\mathcal{C}$, $\boldsymbol{n}_s$ is a unit vector normal to the curve $\mathcal{C}$ at $\boldsymbol{r}_s$, and $\boldsymbol{e}=\boldsymbol{r}/r=(\cos\theta,\sin\theta)$. We define the time-averaged far-field pattern $\bar{\mathcal{F}}(\theta)$ as the angle-dependent part of $\bar{\mathcal{I}}(\boldsymbol{r},t)$, i.e.,

$$\bar{\mathcal{F}}(\theta)=\int d\omega \lim_{T\to\infty}\frac{2\pi}{T}|f_T(\theta,\omega)|^2. \tag{6}$$

In Fig. 3(a), we plot $\bar{\mathcal{F}}(\theta)$ for the stationary lasing solution of the SB model. One can see a strikingly good agreement between the result from the SB model and that from the ray model. It is remarkable that the far-field pattern of the SB model reproduces not only the highest peaks, but also the tiny ones at $\theta\approx 5°$, 175°, 185°, and 355°. The magnification of the first quadrant is shown in Fig. 3(b), where the results for the cavity sizes $r=33.88$ and 16.94 are also presented. Since the increase of the r value results in the decrease of the wavelength, one can see that the larger the r value, the shorter the spatial oscillation period becomes. Nevertheless, if we average out the oscillations, all these far-field patterns show a similar trend with a peak at around $\theta=30°$. This

invariance of the peak position with respect to the change of the cavity size convinces us that our system with $r=67.77$ is well inside the semiclassical regime.

We note that besides the present study for $a/r=6/7$, we performed numerical simulations of the SB model for various a/r values ranging from 0.13 to 1.4 while the other parameters are set to be the same values as those used in this paper. For relatively large a/r values, we could confirm a good ray-wave correspondence. A detailed study on the condition for the good ray-wave correspondence will be reported elsewhere.

One natural approach to explain the appearance of the emission directionality in the SB model is based on the study of the cold-cavity modes. Analyzing the power spectrum for the electric field of the lasing solution for $r=67.77$, we confirmed that it consists of multiple lasing modes, with the major contribution being from six lasing modes, and these all exhibit strong far-field emission at $\theta\approx 30°$, 150°, 210°, and 330°. From this result, we can infer that cold-cavity modes with the above directionality are preferentially excited. To investigate the origin of this mode selection, we study below the cold-cavity modes, focusing on the dependence of the emission directionality upon the Q value, which is one of the important factors for the mode selection.

In the SB model, a cold-cavity mode $E(x,y,t)=e^{-i\xi t}\psi(x,y)$ $(\xi\in\mathbb{C})$ is a solution of Eq. (1) with $\alpha=\mu=0$. Namely, $\psi(x,y)$ satisfies $\left(\nabla^2+\frac{n^2}{n_{in}^2}+2\xi\right)\psi(x,y)=0$. We plot in Fig. 4(a) the far-field pattern of a cold-cavity mode having strong far-field emission at $\theta\approx 30°$. In the gain band of our simulation, i.e., $|\mathrm{Re}\ \xi|\leq 0.01$, we find 98 cold-cavity modes numerically. As Figs. 4(b) and 4(c) show, there also exist cold-cavity modes whose far-field patterns are less or even not similar with that of the ray model. Such modes, however, turn out to have lower Q values as we see below.

To quantify the far-field emission strength around $\theta=30°$, we compute the quantity $\chi=\int_{20}^{40}\mathcal{I}(\theta)d\theta/\int_{0}^{90}\mathcal{I}(\theta)\,d\theta$, where $\mathcal{I}(\theta)$ is the far-field pattern of the cold-cavity mode. Plotting χ-values as a function of the loss rates $-\mathrm{Im}\ \xi$ as shown in Fig. 5, we find a clear tendency that the lower the loss rate, the stronger the far-field emission at $\theta\approx 30°$. In other words, at least in this case the directional modes based on the unstable manifolds also correspond to the high-Q modes and are thus preferentially selected for lasing, while in general we expect that other factors besides the Q value will come into the mode selection, such as mode volume and spatial hole-burning effects.

We note that recently Lebental *et al.* have succeeded in experimentally observing highly directional emission for a polymer stadium cavity with the aspect ratio $a/r=0.8$ [19]. In the experiment, strong far-field emission has been observed at $\theta\approx 30°$, 150°, 210°, and 330°, which agrees with our numerical results shown in Fig. 3, although the aspect ratio for the numerical simulation $(a/r=6/7)$ is slightly different from $a/r=0.8$. Carrying out numerical simulations of the SB model also for $a/r=0.8$, we checked that this slight difference of the cavity geometry does not cause a significant change in the peak position of the far-field pattern; the peaks are shifted by only about 2°. A conspicuous difference between the numerical and experimental far-field data is that one of the peaks in the experimental data (Fig. 4 in Ref. [19]) has a three times larger intensity than the other three peaks. This is however, due to the lifetime effect of the laser dye used in the experiment.

In summary, we demonstrated via numerical simulations of the nonlinear lasing equations that the stadium-cavity laser exhibits a highly directional emission pattern in good agreement with the ray model, which predicts emission directionality based on the geometry of the unstable manifolds of short periodic orbits. Furthermore, we confirmed that for the stadium in this parameter range all of the high-Q modes exhibit this high-emission directionality. Further analysis is needed to elucidate to what extent this property of the high-Q modes holds when one changes the refractive index value, cavity size, cavity shape, and so on.

We acknowledge helpful discussions with Harald G.L. Schwefel and Satoshi Sunada. The work at ATR was supported in part by the National Institute of Information and Communication Technology of Japan. The Yale portion of this work was supported by the National Science Foundation under Grant No. 0408638.

[1] M. C. Gutzwiller, *Chaos in Classical and Quantum Mechanics* (Springer, Berlin, 1990); H. J. Stockmann, *Quantum Chaos: An Introduction* (Cambridge University Press, Cambridge, England, 1999).
[2] J. U. Nöckel, A. D. Stone, and R. K. Chang, Opt. Lett. **19**, 1693 (1994).
[3] J. U. Nöckel, A. D. Stone, G. Chen, H. L. Grossman, and R. K. Chang, Opt. Lett. **21**, 1609 (1996).
[4] J. U. Nöckel and A. D. Stone, in *Optical Processes in Microcavities*, edited by R. K. Chang and A. J. Campillo (World Scientific, Singapore, 1996).
[5] J. U. Nöckel and A. D. Stone, Nature (London) **385**, 45 (1997).
[6] C. Gmachl, F. Capasso, E. E. Narimanov, J. U. Nöckel, A. D. Stone, J. Faist, D. L. Sivco, and A. Y. Cho, Science **98**, 1556 (1998).
[7] N. B. Rex, H. E. Tureci, H. G. L. Schwefel, R. K. Chang, and A. D. Stone, Phys. Rev. Lett. **88**, 094102 (2002).
[8] H. G. L. Schwefel, N. B. Rex, H. E. Tureci, R. K. Chang, A. D. Stone, T. B. Messaoud, and J. Zyss, J. Opt. Soc. Am. B **21**, 923 (2004).
[9] M. Hentschel and M. Vojta, Opt. Lett. **26**, 1764 (2001).
[10] T. Fukushima and T. Harayama, IEEE J. Quantum Electron. **10**, 1039 (2004).
[11] L. A. Bunimovich, Commun. Math. Phys. **65**, 295 (1977).
[12] S.-Y. Lee, S. Rim, J.-W. Ryu, T.-Y. Kwon, M. Choi, and C.-M. Kim, Phys. Rev. Lett. **93**, 164102 (2004).
[13] S.-Y. Lee, J.-W. Ryu, T.-Y. Kwon, S. Rim, and C.-M. Kim,

Phys. Rev. A **72**, 061801(R) (2005).
[14] J.-W. Ryu, S.-Y. Lee, C.-M. Kim, and Y.-J. Park, Phys. Rev. E **73**, 036207 (2006).
[15] T. Harayama, P. Davis, and K. S. Ikeda, Phys. Rev. Lett. **90**, 063901 (2003).
[16] T. Harayama, T. Fukushima, S. Sunada, and K. S. Ikeda, Phys. Rev. Lett. **91**, 073903 (2003).
[17] S. Sunada, T. Harayama, and K. S. Ikeda, Phys. Rev. E **71**, 046209 (2005).
[18] T. Harayama, S. Sunada, and K. S. Ikeda, Phys. Rev. A **72**, 013803 (2005).
[19] M. Lebental, J. S. Lauret, R. Hierle, and J. Zyss, Appl. Phys. Lett. **88**, 031108 (2006).